Supporting Information

Self-destructive PEG-BODIPY nanomaterials for photodynamic and photothermal therapy

Chaonan Li,[a,b] Wenhai Lin, [a,c] Shi Liu,[a] Wei Zhang*[a,c] and Zhigang Xie*[a,b]

Table of Contents

1. Experimental Section

2. Scheme S1. Synthetic route of BDP and I-BDP

3. Figure S1. MALDI-TOF mass (a, c) and ^{1}H NMR spectrum (b, d) of PEG-BDP and PEG-IBDP, respectively.

4. Figure S2. The size distribution measured by DLS of PEG-BDP NPs (a) and PEG-IBDP NPs (b). Stability of PEG-BDP NPs and PEG-IBDP NPs in water (c) and 10% FBS (d).

5. Figure S3. Linear time data versus -ln θ obtained from the cooling period of PEG-BDP NPs (a) and PEG-IBDP NPs (b). Multiple temperature rise and fall cycle curves of PEG-BDP NPs (c) and PEG-IBDP NPs (d) under 685nm laser irradiation (0.55 W cm^{-2}) for four times light on/off.

6. Figure S4. Singlet oxygen production ability of the molecule and NPs. The absorption spectra of DPBF with PEG-BDP molecule (a) and PEG-IBDP molecule (b) in DMF after irradiation with a 685 nm laser (7 mW cm^{-2}) from 0 to 70 s. The absorption spectra of ABDA with PEG-BDP NPs (c) and PEG-IBDP NPs (d) in PBS after irradiation with a 685 nm laser (136 mW cm^{-2}) from 0 to 140 s.

7. Figure S5. (a) Mass spectrometric analysis images of PEG-IBDP molecules after 12 h illumination and the inset image with and without illumination. (b) The zeta potential of PEG-IBDP NPs in water with or without illumination. (c) Absorbance of PEG-IBDP@r-BDP NPs without illumination and original solution.

8. Figure S6. CLSM images of co-stained with PEG-BDP NPs and PEG-IBDP NPs and Lyso-Tracker Green in HeLa cell. Fluorescence images: nuclei (blue), Lyso-Tracker (green), NPs (red) and merged images from top to bottom. Scale bar, 20μm.

9. Figure S7. Fluorescence images of live (green, stained with AM) and dead (red, stained with PI) with HeLa cells after incubating with PEG-BDP NPs and PEG-IBDP NPs (0.25-10 μM) and irradiation with 685 nm laser (0.55 W cm^{-2}) for 5 min. Scale bar, 20 μm.

10. Figure S8. Imaging properties of PEG-BDP NPs. PA images (a) and PA signal intensity of PEG-BDP NPs with different concentrations. PA images (c) and NIRF images (d) of tumor tissues in vivo after tail vein injection of PEG-BDP NPs at different time. Tumors are drawn in white circles.

11. **Figure S9.** NIRF imaging of PEG-BDP NPs (a, c) and PEG-IBDP NPs (b, d) by intratumoral

injection at different time.

12. **Figure S10.** Quantitative PA signal intensity (a, d) and fluorescence intensity (b, e) of tumor site after vein injection of nanoparticles. Quantitative fluorescence intensity of tumor site after intratumoral injection of PEG-BDP NPs (c) and PEG-IBDP NPs (f).

13. **Figure S11.** The structure of r-BDP (left) and g-BDP (right).

Materials. The starting materials Terephthalaldehyde, 4-(Diphenylamino) benzaldehyde and Trifluoroacetic acid were purchased from Adamas Reagent Co., Ltd.. Sodium borohydride was bought from Fuchen (Tianjin) chemical reagents Co., Ltd.. 2, 4-Dimethly-1H-pyrrole was purchased from Suzhou Boke Chemistry Co., Ltd.. 2, 3-dichloro-5, 6-dicyano-1, 4-benzoquinone (DDQ) was purchased from Tianjin Seans Biochemical Technology Co., Ltd.. N-iodosuccinimide (NIS) was purchased from Multipoint Chemical Reagent Co., Ltd.. Boron fluoride ethyl ether (BF_3 EtO_2), Piperidine and acetic acid were purchased from Sinopharm Chemical Reagent Beijing Co., Ltd.. Triethylamine (Et_3N) was brought from Shanghai Aladdin Biochemical Technology Co., Ltd.. $mPEG_{2k}$ was purchased from Sigma-Aldrich (Shanghai) Trading Co., Ltd.. 4-Dimethylaminopyridine (DMAP) was purchased from Energy Chemical Co., Ltd.. N-(3-Dimethylaminopropyl)-N-ethylcarbodiimide (EDC HCl). Reactive Oxygen Species Assay Kit (DCFH-DA) were obtained from Shanghai Beyotime Biotechnology Co., Ltd.. Lyso-Traker Green was purchased by Dalian Meilun Biotechnology Co., Ltd.. Cells viability (live/dead cell staining) assay kit and Hoechst 33258 were purchased from Jiangsu KeyGEN Biotechnology Co., Ltd.. 3-(4,5-dimethylthiazol-2-yl)-2,5-diphenyltetrazolium bromide (MTT) was purchased from Shanghai yanye Bio-Technology Co., Ltd.. TK, g-BDP and r-BDP were synthesized from our groups. Solvents for chemical synthesis were purified by distillation.

Characterizations.

^1H NMR spectra were measured in $CDCl_3$ at room temperature by an AV-400 NMR spectrometer from Bruker. UV and Fluorescence were recorded on SHIMADZU UV-2450 and Edinburgh Instrument FLS-920 spectrometer, respectively. Diameter, diameter distribution of the nanoparticles were determined by Malvern Zeta-sizer Nano for dynamic light scattering (DLS). The measurement was carried out at 25 ^oC and the scattering angle was fixed at 90^o. The morphology of the nanoparticles was measured by transmission electron microscopy (TEM) performed on a JEOL JEM-1011 electron microscope operating at an acceleration voltage of 100 kV. To prepare specimens for TEM, a drop of NPs solution (0.1 mg mL^{-1}) was deposited onto a copper grid with a carbon coating. The specimens were air-dried and measured at room temperature. Confocal laser scanning microscopy (CLSM) images were taken using a Zeiss LSM 700 (Zurich, Switzerland). Flow cytometry was carried out on Guava easyCyte 6-2LBase System (Merck Millipore, USA). MTT assays were measured at 490 nm by a microplate reader (BioTek,

EXL808).

Synthesis of 4-(hydroxymethyl) benzaldehyde. Terephthalaldehyde (2 g, 15.3 mmol) was dissolved in a mixture of ethanol (CH_3CH_2OH) (25 mL) and tetrahydrofuran (THF) (35 mL), then sodium borohydride ($NaBH_4$) (4.5 mmol) was added and stirred in ice bath for 6 hours. After the reaction, the pH value of the mixed solution was adjusted to about 5 by adding hydrochloric acid solution (2 M) drop by drop. The organic layer was collected by extraction with ethyl acetate and water after drying, and finally purified by chromatography silica gel column. The final product was a transparent liquid. Yield: 83%. ^{1}H NMR (400 MHz, $CDCl_3$) δ=10.02 (s, 1H), 7.87 (d, J=8.3 Hz, 2H), 7.53 (d, J=6.6 Hz, 2H), 4.82 (s, 2H).

Synthesis of the (4-(5,5-difluoro-1,3,7,9-tetramethyl-5H-4l4,5l4-dipyrrolo[1,2-c:2',1'-f][1,3,2]diazaborinin-10-yl)phenyl)methanol (Bodipy 1). 4-(hydroxymethyl)benzaldehyde (10 mmol) was dissolved in dried dichloromethane (400 mL) and 2,4-dimethyl-1H-pyrrole (22 mmol) was added under N_2 protection, and then trifluoroacetic acid was added. After stirring at room temperature for a period of time, DDQ (10 mmol) was added and continue stirring for 2 hours. Slowly add NEt_3 (10 mL) and $BF_3{\cdot}Et_2O$ (12 mL) and continue stirring for 2 h. The mixed solution was washed by water, the organic layer was dried and concentrated on a rotary evaporator, and finally purified by chromatography silica gel column. The product was a yellow solid. Yield: 20%. ^{1}H NMR (400 MHz, $CDCl_3$) δ=7.49 (d, J=8.0Hz, 2H), 7.28 (d, J=8.1Hz, 2H), 5.98 (s, 2H), 4.82 (d, J=5.8 Hz, 2H), 2.56 (s, 6H), 1.38 (s, 6H).

Synthesis of the Bodipy 1-I. Bodipy 1 (354 mg, 1 mmol) and NIS (900 mg, 4 mmol) were added in dry CH_2Cl_2 (40 mL). The mixed solution stirred after 4 hours at room temperature and then concentrated on a rotary evaporator. The final product was purified by a silica gel column. The product was a red solid. Yield: 70%. ^{1}H NMR (400 MHz, $CDCl_3$) δ=7.53 (d, J=8.1Hz, 2H), 7.25 (d, J=6.6Hz, 2H), 4.84 (d, J=5.8 Hz, 2H), 2.65 (s, 6H), 1.39 (s, 6H).

Synthesis of the Bodipy 2 and 2-I. Bodipy 1 (0.56 mmol) or Bodipy 1-I (0.56 mmol) and 4-(diphenylamino)benzaldehyde (1.68 mmol) are added in toluene (30 mL), followed by a small amount of piperidine and acetic acid. The mixed solution was heated to 125 ^{o}C for 2 hours under the protection of N_2. The final product was purified by a silica gel column. The Bodipy 2 was a blackish green solid and Bodipy 2-I was a navy blue solid. Yield: 24%. ^{1}H NMR (400 MHz, $CDCl_3$) of Bodipy 2, δ=7.60 (d, *J*=16.2 Hz, 2H), 7.49 (d, *J*=8.0 Hz, 2H), 7.47 (d, *J*=8.6 Hz, 4H), 7.32

(d, *J*=8.0 Hz, 2H), 7.30–7.26 (m, 8H), 7.21–6.99 (m, 18H), 6.60 (s, 2H), 4.82 (d, *J*=5.8 Hz, 2H), 1.43 (s, 6H). MALDI-TOF MS: 864.4. ^{1}H NMR (400 MHz, $CDCl_3$) of Bodipy 2-I δ=8.12 (d, J=16.6Hz, 2H), 7.59 (d, J=16.6 Hz, 2H), 7.52 (dd, J=11.8, 8.4 Hz, 6H), 7.31–7.26 (m, 10H), 7.14 (d, J=7.7 Hz, 8H), 7.07 (dd, J=14.3, 7.9 Hz, 8H), 4.85 (d, J=5.7 Hz, 2H), 1.44 (s, 6H). MALDI-TOF MS: 1116.2.

Synthesis of the TK-PEG$_{2K}$. TK (126 mg, 0.5 mmol) and mPEG$_{2k}$ (200 mg, 0.1 mmol) were added in dry CH_2Cl_2 (30 mL), then EDC·HCl (36 mg, 0.2 mmol) and DMAP (1.2 mg, 0.01 mmol) were added in mixture solution. After 24 hours of stirring at room temperature, the solution was concentrated and dripped into ice ether. After centrifugation and drying, white solid products were obtained. Yield: 25%. ^{1}H NMR (400 MHz, DMSO) δ=3.71–3.31 (m, 180H), 3.24 (s, 3H), 2.75 (dd, J=15.4, 7.3 Hz, 4H), 2.63 (dd, J=18.4, 11.5 Hz, 4H).

Synthesis of the PEG-BDP and PEG-IBDP. Bodipy 2 (30 mg, 0.035 mmol) or 2-I (40 mg, 0.035 mmol) and TK-PEG$_{2K}$ (80 mg, 0.035 mmol) were added in dry CH_2Cl_2 (30 mL), then EDC·HCl (12.6 mg, 0.07 mmol) and DMAP (0.43 mg 0.0035 mmol) were added in mixture solution. After 24 hours of stirring at room temperature, the solution was concentrated. The final product was purified by a silica gel column. The PEG-BDP was a blackish green solid and PEG-IBDP was a navy blue solid. Yield: 40% and 35%, respectively. ^{1}H NMR (400 MHz, $CDCl_3$) of PEG-BDP. δ=7.60 (d, *J*=16.2 Hz, 2H), 7.48 (t, J=8.1 Hz, 6H), 7.34–7.25 (m, 10H), 7.21–7.00 (m, 18H), 6.61 (s, 2H), 5.24 (s, 2H), 3.71–3.59 (m, 180H), 3.38 (s, 3H), 2.89 (dd, J=15.8, 7.5 Hz, 4H), 2.69 (dt, J=29.4, 7.3 Hz, 4H), 1.61 (s, 6H), 1.43 (s, 6H).

^{1}H NMR (400 MHz, $CDCl_3$) of PEG-IBDP. δ=8.12 (d, J=16.6 Hz, 2H), 7.58 (d, J=16.6 Hz, 2H), 7.52 (dd, J=11.8, 8.4 Hz, 6H), 7.31–7.26 (m, 10H), 7.14 (d, J=7.7 Hz, 8H), 7.07 (dd, J=14.3, 7.9 Hz, 8H), 5.26 (s, 2H), 3.72–3.53 (m, 180H), 3.38 (s, 3H), 2.91 (dt, J=21.0, 7.3 Hz, 4H), 2.70 (dt, J=38.2, 7.3 Hz, 4H), 1.62 (s, 6H), 1.44 (s, 6H).

Preparation of PEG-BDP NPs and PEG-IBDP NPs. Nanoparticles were prepared by precipitation method. First, the PEG-BDP compound and PEG-IBDP compound were dissolved in THF and the solution was slowly dripped into the pure water stirred at a uniform speed. Second, liquid were collected and dialyzed after complete volatilization of THF. Finally, the dialysate was centrifuged to obtain uniformly dispersed nanoparticles. The concentration of nanoparticles was determined by measuring ultraviolet absorption.

In vitro Photothermal effects. PEG-BDP NPs and PEG-IBDP NPs in water with different

concentration (7.5-50 μg mL^{-1}) was irradiated under 685 nm laser (0.55 W cm^{-2}, 5 min). PEG-BDP NPs and PEG-IBDP NPs in water with different laser intensity (0.38 W cm^{-2}, 0.55 W cm^{-2}, 0.76 W cm^{-2}) were irradiated with 685 nm laser for 5 min. The photothermal response of PEG-BDP NPs and PEG-IBDP NPs in water (30 μg mL^{-1}, 200 μL) was recorded with laser irradiation (685 nm, 0.55 W cm^{-2}, 5 min) and then shut off. The cycling heating-cooling curves were investigated with 685 nm laser irradiation (0.55 W cm^{-2}). All temperatures were recorded every 10s. The photothermal images were obtained by near-infrared thermal imaging instrument. The photothermal conversion efficiency (η) was calculated according to the equation (Eq) as follows according to published methods.[RS1] $$\eta = \frac{h\,A\,\Delta T_{max} - Q_s}{I\,(1 - 10^{-A_\lambda})}$$ (1), where h is the heat transfer coefficient, A is the surface area of the container, ΔT_{max} is the maximum temperature change, I is the laser power, A_λ is the absorbance at 685 nm, Q_s is the heat associated with the light absorbance of the solvent. In to get the $h\,A$, θ defined as the ratio of ΔT to ΔT_{max} was introduced : $\theta = \frac{\Delta T}{\Delta T_{max}}$. Based on the total energy balance for this system: $$\sum_i m_i\,C_{p,i}\frac{dT}{dt} = Q_{NPs} + Q_s - Q_{loss}$$ (2), where Q_{NPs} is the photothermal energy input by NPs, Q_s is the heat associated with the light absorbance of the solvent, Q_{loss} is thermal energy lost to the surroundings. At the maximum steady-state temperature, the heat input is equal to the heat output: $Q_{NPs} + Q_s = Q_{loss} = h\,A\,\Delta T_{max}$. Substituting θ into Eq.2 and rearranging: $$\frac{d\theta}{dt} = \frac{h\,A}{\sum_i m_i\,C_{p,i}}\left(\frac{Q_{NPs} + Q_s}{h\,A\,\Delta T_{max}} - \theta\right)$$ (3), When the laser was shut off, the $Q_{NPs} + Q_s = 0$, Eq.3 changed to: $$dt = -\frac{\sum_i m_i\,C_{p,i}}{h\,A}\frac{d\theta}{\theta}$$ (4). Integrating Eq.4 gives the expression: $t = -\frac{\sum_i m_i\,C_{p,i}}{h\,A}\theta$. Then $h\,A$ can be determined by applying the linear time data from the cooling period versus $-Ln\theta$.

The capacity of ROS generation. The ability of PEG-IBDP molecule in DMF to produce ROS in vitro were obtained by the change of absorption intensity of DPBF at 415 nm. DPBF solution (20 μL, 1 mg mL^{-1}) was added to PEG-IBDP solution and the absorption of DPBF solution was measured after a specific time of illumination with 685 nm laser at 50 mW cm^{-2}. The detection

interval was 10 s. The ability of PEG-IBDP NPs in water to produce ROS in vitro was obtained by the change of absorption intensity of ABDA at 380 nm. ABDA solution (70 μL, 1mg mL^{-1}) was added to PEG-IBDP NPs and the absorption of ABDA solution was measured after a specific time of illumination with 685 nm laser at 136 mW cm^{-2}. The detection interval was 20 s. The same tests were done with PEG-BDP as control.

ROS-triggered the destruction of PEG-IBDP NPs in vitro. We encapsulated r-BDP into the PEG-IBDP NPs and formed PEG-IBDP@r-BDP NPs. The biological environment was simulated with buffer solution of pH=7.4 and the cell membrane was simulated with dialysis bag. The absorbance of PEG-IBDP@r-BDP NPs was measured after 685 nm laser irradiation (0.55 W cm^{-2}) at different time.

Cell lines and cell culture. HeLa cells and HepG2 cells were purchased from the Institute of Biochemistry and Cell Biology, Chinese Academy of Sciences, Shanghai, China. All the cells were grown in Dulbecco's modified Eagle's medium (DMEM, GIBCO) supplemented with 10% heat-inactivated fetal bovine serum (FBS, GIBCO), 100 U mL^{-1} penicillin and 100 μg mL^{-1} streptomycin (Sigma), and the culture medium was replaced once very day. All the cells were cultured in a humidified incubator at 37°C with 5% CO_2.

Cell uptake by confocal laser scanning microscopy (CLSM) and flow cytometry (FCM). Intracellular endocytosis of PEG-BDP NPs and PEG-IBDP NPs was visualized by CLSM. HeLa cells were inoculated into 6-well culture plates (one sterile cover sheet per well), and the number of cells per well was 5×10^4 cells. After 24 hours cultured, the PEG-BDP NPs and PEG-IBDP NPs (5 μM, diluted with DMEM) were used to culture the cells at predetermined time points. After incubation, the supernatant was removed and the cells were washed with PBS. Subsequently, the cells were immersed in 4% formaldehyde (1 mL) to each well at room temperature. After ten minutes, cells were washed twice with PBS. The nuclei were then stained with Hoechst 33258. Slides were mounted and viewed using a confocal laser scanning microscope imaging system.

Flow cytometry was used to quantitatively analyze the time-dependent endocytosis. HeLa cells were inoculated into 6-well culture plates, and the number of cells per well was 5×10^4 cells. After 24 hours cultured, the PEG-BDP NPs and PEG-IBDP NPs (5 μM, diluted with DMEM) were used to culture the cells at different time points. After incubation, the supernatant was removed and the cells were washed with PBS. The cells were digested with 0.5 mL trypsin in each pore and

centrifuged. After centrifugation, the supernatant was discarded and 0.5 mL PBS was added to blow the cells evenly. The final cell suspension analyses by Guava easyCyte 6-2L Base System (Merck Millipore, USA).

Co-localization of lysosomes and PEG-BDP NPs and PEG-IBDP NPs. HeLa cells were incubated with PEG-BDP NPs and PEG-IBDP NPs (5 μM) for 2 h, then the supernatant was removed and the cells were washed with PBS. Subsequently, the cells were immersed in 4% formaldehyde (1 mL) to each well at room temperature. After ten minutes, cells were washed twice with PBS. and stained with Lyso-Tracker Green for 1h and washed twice with PBS. The nuclei were stained with Hoechst 33258. Samples were examined by CLSM.

Intracellular ROS detection. The production of ROS in cells was observed by CLSM. HeLa cells were inoculated into 24-well culture plates (one sterile cover sheet per well), and the number of cells per well was 10^4 cells. After 24 hours of culture, the PEG-BDP NPs and PEG-IBDP NPs (5 μM, diluted with DMEM) were used to culture the cell for 4 hours. Subsequently, the light group was irradiated with 685 nm laser (0.55 W cm^{-2}, 5 min), and the dark group was not treated as the control group. Then, the supernatant was sucked out and the DCFH-DA solution diluted with serum-free DMEM was added. The orifice plate was placed at 37 ^oC and incubated for 30 minutes. Fluorescent pictures of DCF induced by the generation of ROS were observed through CLSM.

Intracellular ROS-triggered the destruction of PEG-IBDP NPs. The production of ROS could rupture PEG-IBDP NPs was detected on the cellular level by using CLSM. We encapsulated g-BDP into the PEG-IBDP NPs and formed PEG-IBDP@g-BDP NPs. HeLa cells were inoculated into 6-well culture plates (one sterile cover sheet per well), and the number of cells per well was 5×10^4 cells. After 24 hours of culture, the PEG-IBDP@g-BDP NPs (the concentration of g-BDP=5 μg mL^{-1}, diluted with DMEM) were used to culture the cells at 0.5 h and 2 h. After incubation, each group of cells was irradiated with 20 mW cm^{-2} for 5 minutes and then incubated for 0.5 h and 2 h, respectively. The sheet was processed according to the above treatment method and observed with CLSM. The same tests were done with BDP as control.

Cytotoxicity assays. In order to evaluate the phototoxicity (toxicity of laser irradiation) and biocompatibility (toxicity of no laser irradiation) of PEG-BDP NPs and PEG-IBDP NPs in vitro, HeLa and HepG2 cells were tested for cell viability by MTT assay. Cells were inoculated into 96-

well culture plates, and the number of cells per well was 10^4 cells. After 24 hours of culture, the PEG-BDP NPs and PEG-IBDP NPs of different concentration were used to incubate the cells and four parallel holes were used for each sample concentration. After incubation for 4 hours, cells in light group were irradiated with a 685 nm laser at 0.55 W cm^{-2} for 5 minutes and in dark group were placed in the same environment without light for 5 minutes. After 24 hours of incubation, 20 μL MTT solution (5mg mL^{-1}) was added to each orifice plate. After 4 hours, the supernatant was sucked out and 150 mL DMSO was added. The orifice plate was shocked for 3 minutes and the absorption value at 490 nm was detected by a Bio-Rad 680 microplate reader.

Live and dead cell staining assays. In order to visualize the phototoxicity of PEG-BDP NPs and PEG-IBDP NPs in vitro, HeLa cells were stained with PI and AM. First, Cells were incubated with PEG-BDP NPs and PEG-IBDP NPs of different concentration. Second, cells in light group were irradiated with a 658 nm laser at 0.55 W cm^{-2} for 5 minutes and in dark group were placed in the same environment without light for 5 minutes. After 24 hours of incubation, the cells were stained with AM and PI at room temperature for 30 minutes. Subsequently, the staining solution was sucked out and cells were washed by PBS. Finally, the cells were imaged by a Nikon C1si laser scanning confocal microscopy. In the picture, green represented living cells and red represented dead cells.

In vitro and vivo PA imaging of PEG-BDP NPs and PEG-IBDP NPs. In vitro and in vivo PA imaging experiments were all performed using the reported methods.[RS2] For in vivo PA imaging, PEG-BDP NPs and PEG-IBDP NPs (5.0 mg kg^{-1}) was injected into mice by intravenous injection. PA images were acquired and the results were analyzed via ViewMOST software.

Kunming strain female mice (about 20 g) were purchased from Jilin University, China, and cared in an ethical and humane way. All the experiments were performed in strict accordance with the NIH guidelines for the care and use of laboratory animals (NIH Pub-lication No. 85-23 Rev. 1985). All protocols were approved by the guidelines of the Committee on Animal Use and Care of Chinese Academy of Sciences.

In vivo NIRF imaging and bio-distribution of PEG-BDP NPs and PEG-IBDP NPs. The PEG-BDP NPs and PEG-IBDP NPs liquid (5.0 mg kg^{-1}) was injected into mice by intravenous and intratumoral injection. The fluorescence imaging of mice was obtained by the Meatro 500 FL in vivo optical imaging system (Cambridge Research & Instrumentation, Inc. USA), in which the

excitation light of the imaging was dark red. Fluorescence imaging of mice at different injection times under the condition of anesthesia.

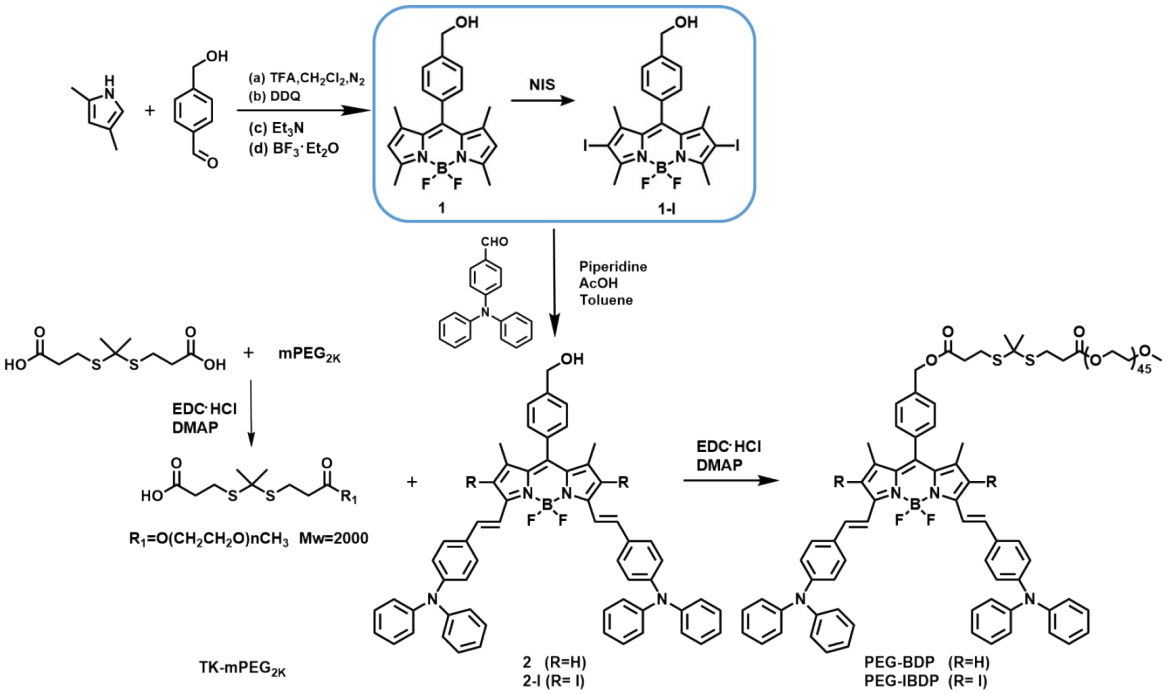

Scheme S1. Synthetic route of PEG-BDP and PEG-IBDP

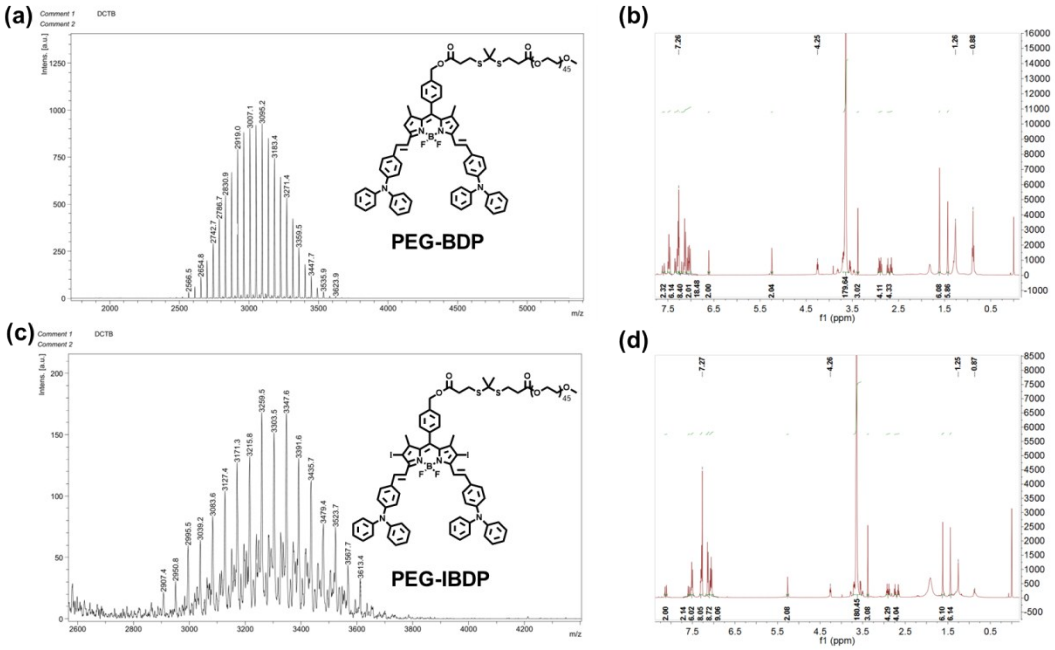

Figure S1. MALDI-TOF mass (a, c) and NMR (b, d) spectrum of PEG-BDP and PEG-IBDP, respectively.

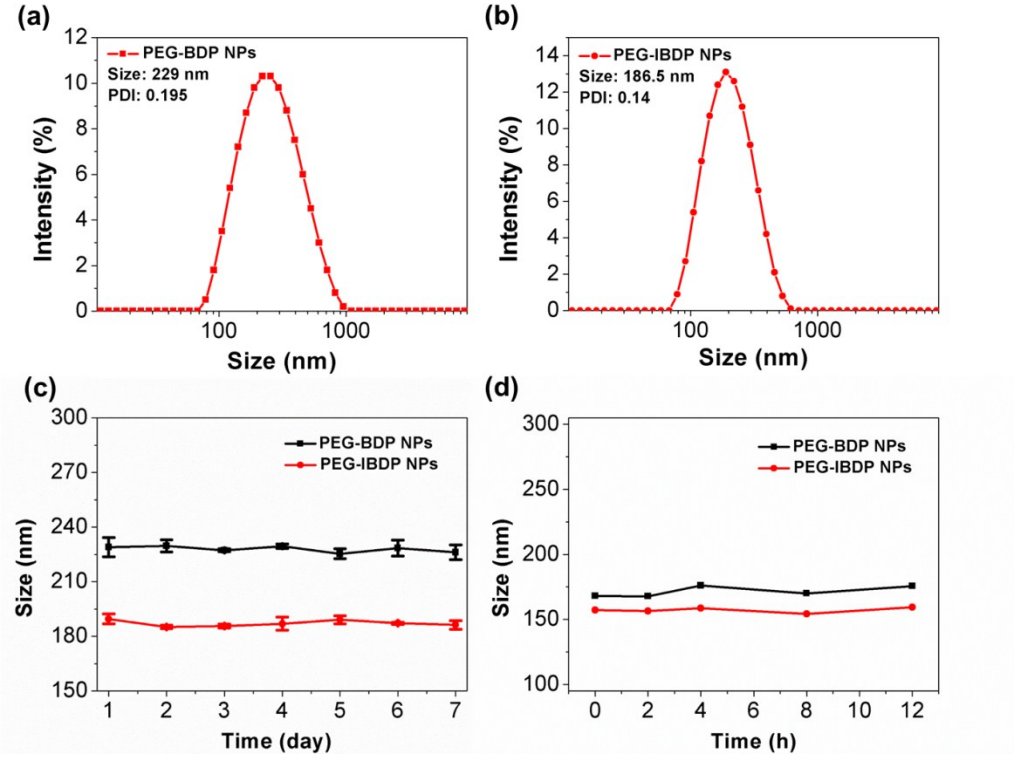

Figure S2. The size distribution measured by DLS of PEG-BDP NPs (a) and PEG-IBDP NPs (b). Stability of PEG-BDP NPs and PEG-IBDP NPs in water (c) and 10% FBS (d).

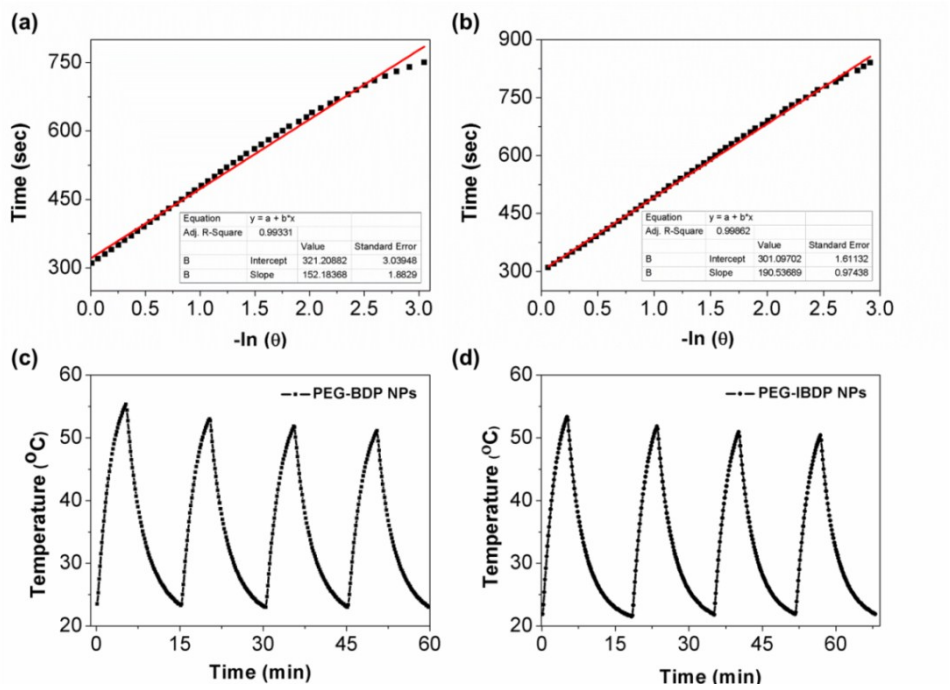

Figure S3. Linear time data versus -ln θ obtained from the cooling period of PEG-BDP NPs (a) and PEG-IBDP NPs (b). Multiple temperature rise and fall cycle curves of PEG-BDP NPs (c) and PEG-IBDP NPs (d) under 685nm laser irradiation (0.55 W cm^{-2}) for four times light on/off.

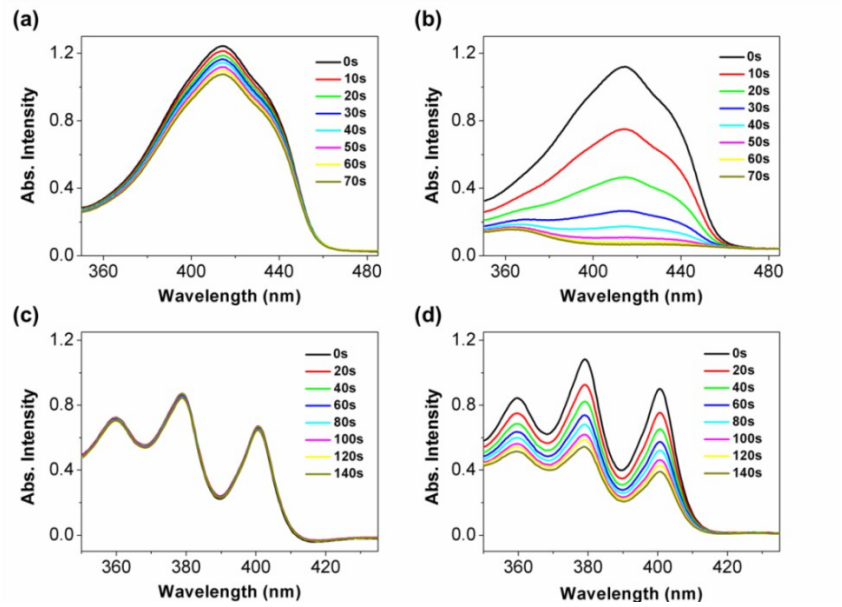

Figure S4. Singlet oxygen production ability of the molecule and NPs. The absorption spectra of DPBF with PEG-BDP molecule (a) and PEG-IBDP molecule (b) in DMF after irradiation with a 685 nm laser (7 mW cm^{-2}) from 0 to 70 s. The absorption spectra of ABDA with PEG-BDP NPs (c) and PEG-IBDP NPs (d) in PBS after irradiation with a 685 nm laser (136 mW cm^{-2}) from 0 to 140 s.

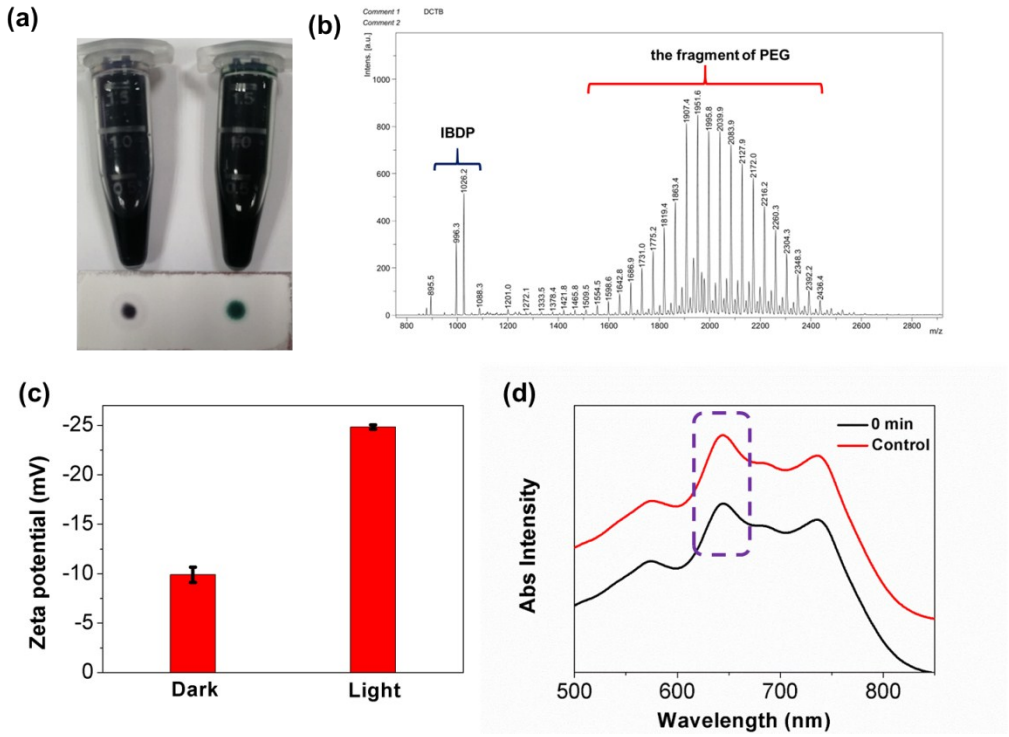

Figure S5. (a) The images of PEG-IBDP molecule in CH2Cl2 with and without NIR irradiation and (b) mass spectrometric analysis of substances after illumination. (c) The zeta potential of PEG-IBDP NPs in water with or without illumination. (d) Absorbance of PEG-IBDP@r-BDP NPs without illumination and original solution.

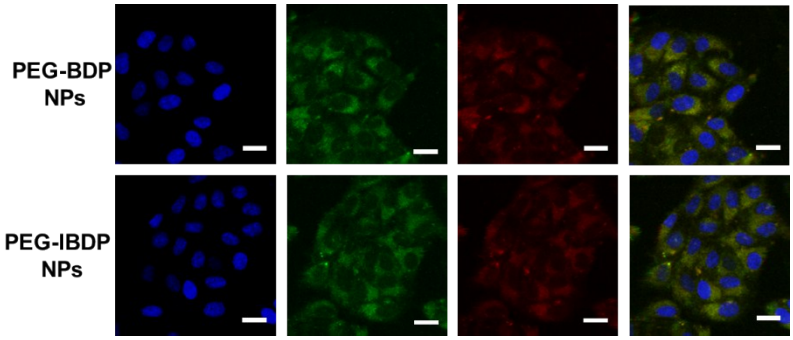

Figure S6. CLSM images of co-stained with PEG-BDP NPs and PEG-IBDP NPs and Lyso-Tracker Green in HeLa cell. Fluorescence images: nuclei (blue), Lyso-Tracker (green), NPs (red) and merged images from top to bottom. Scale bar, 20μm.

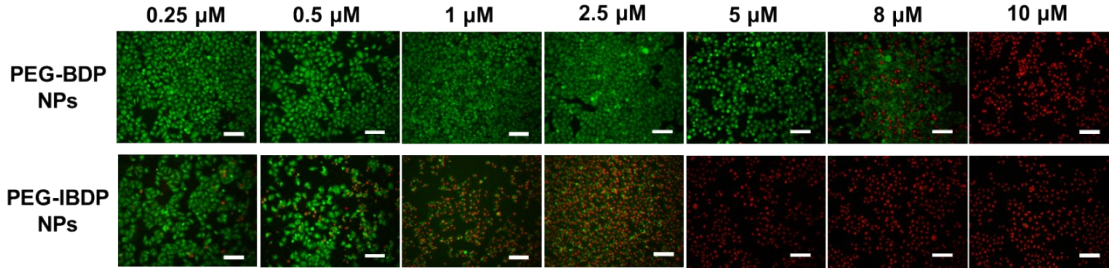

Figure S7. Fluorescence images of live (green, stained with AM) and dead (red, stained with PI)

with HeLa cells after incubating with PEG-BDP NPs and PEG-IBDP NPs (0.25-10 μM) and irradiation with 685 nm laser (0.55 W cm^{-2}) for 5 min. Scale bar, 20 μm.

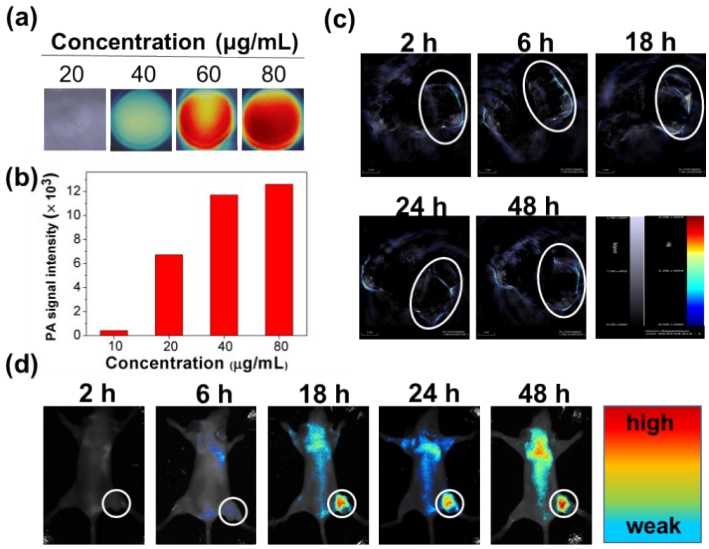

Figure S8. Imaging properties of PEG-BDP NPs. PA images (a) and PA signal intensity of PEG-BDP NPs with different concentrations. PA images (c) and NIRF images (d) of tumor tissues in vivo after tail vein injection of PEG-BDP NPs at different time. Tumors are drawn in white circles.

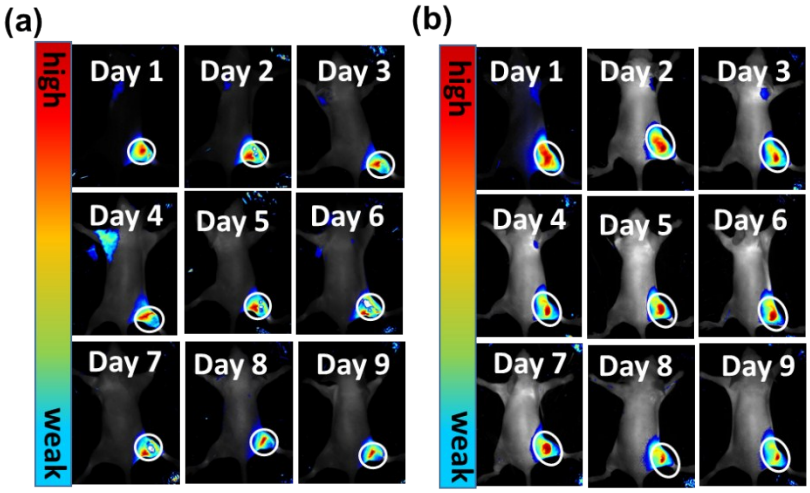

Figure S9. NIRF imaging of PEG-BDP NPs (a) and PEG-IBDP NPs (b) by intratumoral injection at different time.

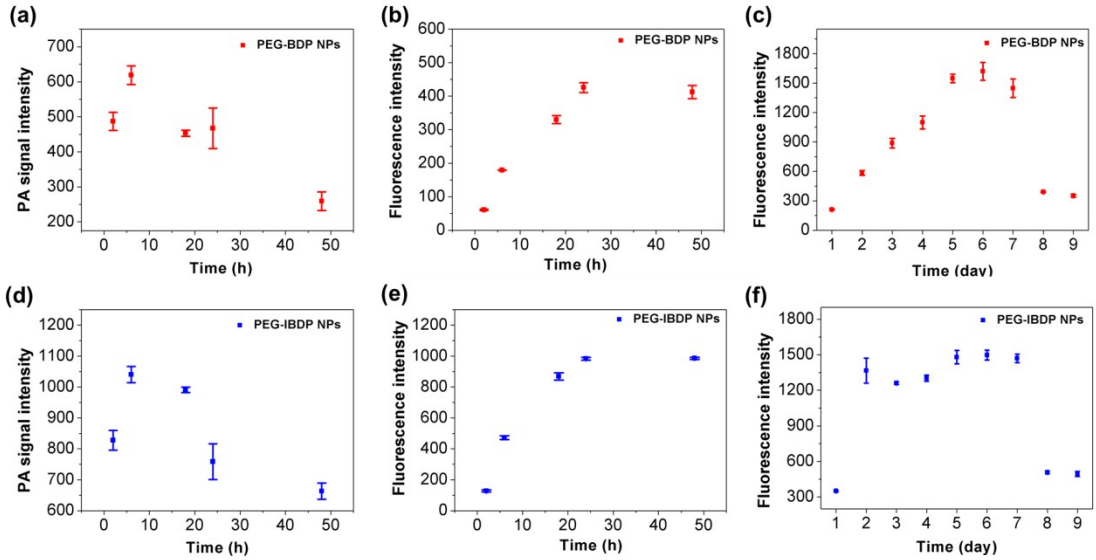

Figure S10. Quantitative PA signal intensity (a, d) and fluorescence intensity (b, e) of tumor site after vein injection of nanoparticles. Quantitative fluorescence intensity of tumor site after intratumoral injection of PEG-BDP NPs (c) and PEG-IBDP NPs (f).

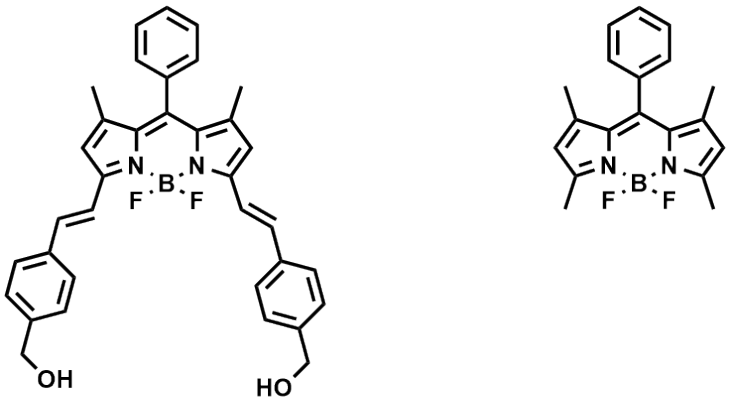

Figure S11. The structure of r-BDP (left) and g-BDP (right).

Reference:

RS1. W. Zhang, W. Lin, X. Wang, C. Li, S. Liu and Z. Xie, ACS Appl. Mater. Interfaces, 2019, 11, 278-287.

RS2. T. Sun, J.-H. Dou, S. Liu, X. Wang, X. Zheng, Y. Wang, J. Pei and Z. Xie, ACS Appl. Mater. Interfaces 2018, 10, 7919-7926.